Electronic Supplementary Information (ESI)

Methylene Insertion into an Fe_2S_2 Cluster: Formation of a Thiolate-Bridged Diiron Complex Containing $Fe-CH_2-S$ Moiety

Linan Su,[a] Dawei Yang,*[a] Yixin Zhang,[a] Baomin Wang[a] and Jingping Qu*[ab]

[a]*State Key Laboratory of Fine Chemicals, Dalian University of Technology, 2 Linggong Road, Dalian 116024, P. R. China*

[b]*Key Laboratory for Advanced Materials, East China University of Science and Technology, Shanghai 200237, P. R. China*

*E-mail: qujp@dlut.edu.cn (J.Q.)
yangdw@dlut.edu.cn (D.Y.)

Contents:

Experimental Section

General Procedures

All manipulations were routinely carried out under a nitrogen atmosphere, using standard Schlenk-line techniques. All solvents were dried and distilled over an appropriate drying agent under argon. Complex $[FeL]_2$ (L = *N*,*N'*-dimethyl-3,6-diazanonane-1,8-dithiolate),[1] $[Cp^*Fe(MeCN)_3][PF_6]$ (Cp* = η^5-C_5Me_5),[2] and $[Cp^*Ru(MeCN)_3][PF_6]$[3] were prepared according to the literatures. $CoCp_2$ (Aldrich) was used without further purification.

Spectroscopic measurements

The ^1H NMR spectra were recorded on a Brüker 400 Ultra Shield spectrometer. Infrared spectra were recorded on a $NEXVS_{TM}$ FT-IR spectrometer. Elemental analyses were performed on a Vario EL analyzer. ESI-HRMS were recorded on a UPLC/Q-Tof micro spectrometer. Solution magnetic susceptibilities were determined by adding an internal capillary standard of the appropriate deuterated solvent to 2-7 mM ^1H NMR samples of metal complexes. The difference between the capillary and solvent peaks in Hz was used to determine μ_{eff} via the Evans method.[4]

X-ray crystallography

The data for complexes **1**, **2**, and **3** were afforded on a Brüker SMART APEX CCD diffractometer with graphite monochromated Mo Kα radiation (λ = 0.71073 Å). Empirical absorption corrections were performed using the SADABS program.[5] Structures were solved by direct methods and refined by full-matrix least-squares based on all data using F^2 using Shelx97.[6] Anisotropic thermal displacement coefficients were determined for all non-hydrogen atoms. Hydrogen atoms were placed at idealized positions and refined with fixed isotropic displacement parameters. Full details of the X-ray structural determination are in the CIF included as Electronic Supplementary Information. CCDC depositions 1434935 (**1**), 1447555 (**2**), 1434939 (**3**) can be obtained free of charge from The Cambridge Crystallographic Data Center.

For **1**, the “simu” restraints were used with the deviation 0.02 to avoid the Hirshfeld Test

Diff on C−N and C−C bonds of N_2S_2 ligand. The "delu" restraints were used with the deviation 0.002 to avoid the Hirshfeld Test Diff on Fe−S bonds. For **2**, the "simu" restraints were used with the deviation 0.01 to avoid the Hirshfeld Test Diff on C−N and C−C bonds of N_2S_2 ligand. The "delu" restraints were used with the deviation 0.001 and 0.01 to avoid the Hirshfeld Test Diff on Fe−S bonds and C−S bonds respectively. The C2−C29 bond distance was fixed 1.40 Å. The "omit" restraints were used on a series of reflections to enhance bond precision on C−C bonds.

Electrochemistry

Electrochemical measurements were recorded using a BAS-100W electrochemical potentiostat at a scan rate of 100 mV/s. Electrochemical experiments were carried out in a three-electrode cell under argon at room temperature. The working electrode was a glassy carbon disk (diameter 3 mm), the reference electrode was a nonaqueous Ag/Ag^+ electrode, the auxiliary electrode was a platinum wire, and the supporting electrolyte was 0.1 M $^{n}Bu_4NPF_6$ in CH_2Cl_2. All potentials reported herein are quoted relative to the $FeCp_2/FeCp_2^+$ couple.

^{57}Fe Mössbauer Spectroscopy

All ^{57}Fe Mössbauer spectroscopy was run on non-enriched solid samples of the as-isolated complexes. Each sample was loaded into a Delrin Mössbauer sample cup for measurements and loaded under liquid nitrogen. Low-temperature ^{57}Fe Mössbauer measurements were performed using a SeeCo MS4 Mössbauer spectrometer integrated with a Janis SVT-400T He/N_2 cryostat for measurements at 80 K. Isomer shifts were determined relative to α-Fe at 298 K. All Mössbauer spectra were fit using the program WMoss (SeeCo).

General computational method

DFT calculations were performed by Gaussian 09 program.[7] The TPSSTPSS functional together with the effective core potentials (ECPs) of Hay and Wadt with double-ζ valence basis sets (LanL2DZ)[8] were chosen to describe Fe atoms and unrestricted density functional theory (UDFT) was used for open-shell system. The 6-31+G(d) basis set was employed for C, S, H, and Cl atoms. No symmetry was adopted in the calculations. Vibrational frequency calculations were performed to ensure that a local minimum has no imaginary frequency. The spin density and molecular orbital analysis were based on the optimized structure at their most stable electronic states.

Preparation of [Cp*Fe(MeCN)LFeCl][PF_6] (1)

[Cp*Fe(MeCN)$_3$][PF_6] (45.9 mg, 0.10 mmol) was added to a suspension of [FeL]$_2$ (L = *N*,*N'*-dimethyl-3,6-diazanonane-1,8-dithiolate) (26.2 mg, 0.05 mmol) in 5 mL MeCN, then 0.5 mL $CHCl_3$ was added at room temperature, the solution color slowly changed from reddish brown to dark green. The reaction mixture was allowed to be stirred for another 2 h. The resulting dark green solution was evaporated to dryness under vacuum, then the greenish black residues were washed with Et_2O (3 × 3 mL) and dried in reduced pressure to obtain a greenish crystalline powder **1** (47.2 mg, 0.07 mmol, 70%). Crystals of **1** suitable for X-ray diffraction experiment were grown from saturated CH_2Cl_2 solution layered by *n*-hexane at room temperature. ^1H NMR (400 MHz, CD_2Cl_2): δ −67.52 (br). μ_{eff} (CD_2Cl_2, 25 °C): 5.66 μ_B. IR (Film; cm^{-1}): 2962, 2915, 2893, 1507, 1491, 1378, 1302, 1261, 1083, 1022, 840, 759, 736, 557. ESI-HRMS: Calcd for [**1**−PF_6−MeCN]$^+$ 488.0474; Found 488.0483. Anal. Calcd for $C_{20}H_{36}S_2N_3Fe_2ClPF_6$: C, 35.60; H, 5.38; N, 6.23. Found: C, 35.73; H, 5.01; N, 5.91.

Preparation of [Cp*Fe(MeCN)L^{CH2}FeCl][PF_6] (2)

[Cp*Fe(MeCN)$_3$][PF_6] (45.9 mg, 0.10 mmol) was added to an orange suspension of [FeL]$_2$ (26.2 mg, 0.05 mmol) in 5 mL CH_2Cl_2 with vigorously stirring at room temperature, then the solution color slowly changed from reddish brown to dark green. The reaction mixture was allowed to be stirred for another 2 h. The resulting dark green solution was evaporated to dryness under vacuum, then the greenish black residues were washed with Et_2O (3 × 3 mL) and dried in reduced pressure to obtain a greenish powder mixture (70% by mass) of **1** (25.6 mg, 0.038 mmol, 38%) and **2** (22.1 mg, 0.032 mmol, 32%). The ratio of **1** and **2** of crystal mixture was determined by ^{57}Fe Mössbauer spectroscopy. Crystals of **2** suitable for X-ray diffraction experiment were grown from saturated CH_2Cl_2 solution layered by *n*-hexane at room temperature. ^1H NMR (400 MHz, CD_2Cl_2): δ 8.47 (br). μ_{eff} (CD_2Cl_2, 25 °C): 4.47 μ_B. IR (Film; cm^{-1}): 2988, 2915, 2259, 1468, 1432, 1379, 1304, 1274, 1076, 1024, 841, 762, 738, 557. ESI-HRMS: Calcd for [**2**−PF$_6$−MeCN]$^+$ 502.0630; Found 502.0613. Anal. Calcd for $C_{21}H_{38}S_2N_3Fe_2ClPF_6$: C, 36.62; H, 5.56; N, 6.10. Found: C, 36.26; H, 5.23; N, 6.04.

Preparation of [Cp*FeClL^{CH2}FeCl] (3)

To a stirred solution of [Cp*Fe(MeCN)LFeCl][PF$_6$] (**1**) (67.5 mg, 0.10 mmol) in 5 mL CH_2Cl_2 was added CoCp$_2$ (22.7 mg, 0.12 mmol) at −78 °C, and followed by slowly elevating to room temperature. Volatiles were removed *in vacuo* and the crude product was extracted with toluene (3 × 3 mL). The red-brown solids **3** (8.1 mg, 0.015 mmol, 15%) were achieved after drying in reduced pressure. Crystals of **3** suitable for X-ray diffraction experiment were grown from saturated toluene solution layered by *n*-pentane at room temperature. ^{1}H NMR (400 MHz, CD_2Cl_2): δ −16.78 (br). μ_{eff} (CD_2Cl_2, 25 °C): 4.36 μ_B. IR (Film; cm^{-1}): 2970, 2906, 2853, 1475, 1427, 1374, 1243, 1093, 1070, 1024, 737. Anal. Calcd for $C_{19}H_{35}S_2N_2Fe_2Cl_2$: C, 42.40; H, 6.56; N, 5.21. Found: C, 42.69; H 6.94; N, 4.97.

Procedure for the reaction of [Cp*Fe(MeCN)$_3$][PF$_6$] with [FeL]$_2$ in CH_2Br_2

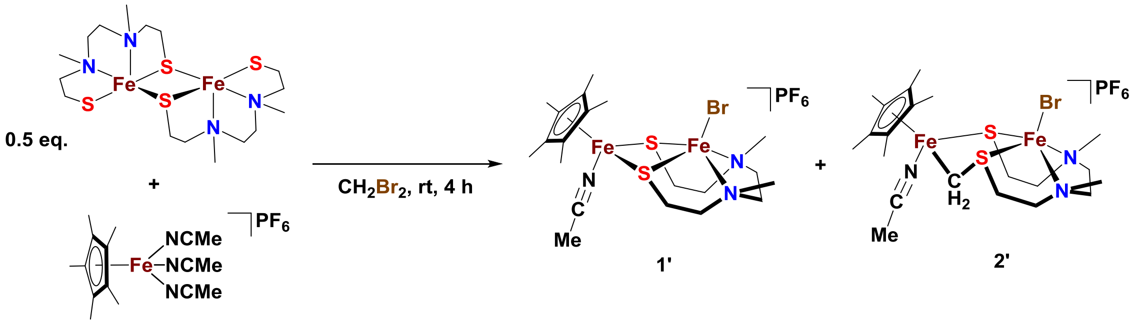

[Cp*Fe(MeCN)$_3$][PF$_6$] (45.9 mg, 0.10 mmol) was added to an orange suspension of [FeL]$_2$ (26.2 mg, 0.05 mmol) in 5 mL CH_2Br_2 with vigorously stirring at room temperature, then the solution color slowly changed from reddish brown to dark green. The reaction mixture was allowed to be stirred for another 2 h. The resulting dark green solution was evaporated to dryness under vacuum, then the greenish black residues were washed with Et$_2$O (3 × 3 mL) and dried in reduced pressure to obtain a greenish powder mixture. ESI-HRMS: Calcd for [**1'**−PF$_6$−MeCN]$^+$ 531.9971; Found 531.9968; [**2'**−PF$_6$−MeCN]$^+$ 546.0127; Found 546.0143.

Procedure for the reaction of [Cp*Ru(MeCN)$_3$][PF$_6$] with [FeL]$_2$ in CH$_2$Cl$_2$

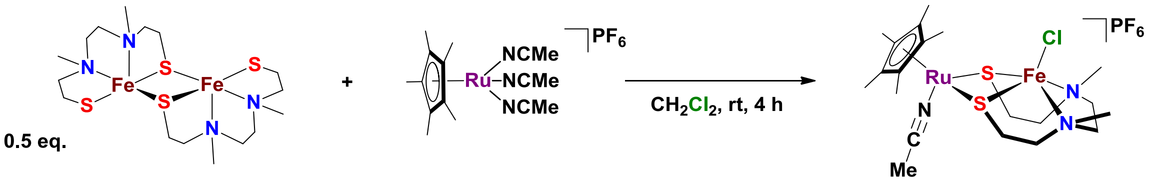

1''

[Cp*Ru(MeCN)$_3$][PF$_6$] (50.4 mg, 0.10 mmol) was added to an orange suspension of [FeL]$_2$ (26.2 mg, 0.05 mmol) in 5 mL CH$_2$Cl$_2$ with vigorously stirring at room temperature, then the solution color slowly changed from reddish brown to yellow. The reaction mixture was allowed to be stirred for another 2 h. The resulting yellow solution was evaporated to dryness under vacuum, then the orange residues were washed with Et$_2$O (3 × 3 mL) and dried in reduced pressure to obtain an orange powder. ESI-HRMS: Calcd for [**1''**−PF$_6$−MeCN]$^+$ 534.0169; Found 534.0164.

References

[1] K. D. Karlin and S. J. Lippard, *J. Am. Chem. Soc.*, 1976, **98**, 6951.

[2] C. Daniel and A. Didier, *Organometallics*, 1984, **3**, 1094.

[3] P. J. Fagan, M. D. Ward and T. C. Calabrese, *J. Am. Chem. Soc.*, 1989, **111**, 1698.

[4] E. M. Schubert, *J. Chem. Educ.*, 1992, **69**, 62.

[5] G. M. Sheldrick, SADABS, Program for area detector adsorption correction, Institute for Inorganic Chemistry, University of Göttingen, Germany, 1996.

[6] (a) G. M. Sheldrick, SHELXL-97, Program for refinement of crystal structures, University of Göttingen, Germany, 1997; (b) G. M. Sheldrick, SHELXS-97, Program for solution of crystal structures, University of Göttingen, Germany, 1997.

[7] Gaussian 09, Revision A.1, M. J. Frisch, G. W. Trucks, H. B. Schlegel, G. E. Scuseria, M. A. Robb, J. R. Cheeseman, G. Scalmani, V. Barone, B. Mennucci, G. A. Petersson, H. Nakatsuji, M. Caricato, X. Li, H. P. Hratchian, A. F. Izmaylov, J. Bloino, G. Zheng, J. L. Sonnenberg, M. Hada, M. Ehara, K. Toyota, R. Fukuda, J. Hasegawa, M. Ishida, T. Nakajima, Y. Honda, O. Kitao, H. Nakai, T. Vreven, J. A. Montgomery, J. E. Jr. Peralta, F. Ogliaro, M. Bearpark, J. J. Heyd, E. Brothers, K. N. Kudin, V. N. Staroverov, R. Kobayashi, J. Normand, K. Raghavachari, A. Rendell, J. C. Burant, S. S. Iyengar, J. Tomasi, M. Cossi, N. Rega, J. M. Millam, M. Klene, J. E. Knox, J. B. Cross, V. Bakken, C. Adamo, J. Jaramillo, R. Gomperts, R. E. Stratmann, O. Yazyev, A. J. Austin, R. Cammi, C. Pomelli, J. W. Ochterski, R. L. Martin, K. Morokuma, V. G. Zakrzewski, G. A. Voth, P. Salvador, J. J. Dannenberg, S. Dapprich, A. D. Daniels, O. Farkas, J. B. Foresman, J. V. Ortiz, J. Cioslowski, D. J. Fox, Gaussian, Inc., Wallingford, CT, 2009.

[8] (a) W. R. Wadt and P. J. Hay, *J. Chem. Phys.*, 1985, **82**, 284; (b) P. J. Hay and W. R. Wadt, *J. Chem. Phys.*, 1985, **82**, 299.

X-ray Crystallographic Information

Table S1. Crystallographic data for **1**, **2** and **3**.

	1	**2**	**3**
Formula	$C_{20}H_{36}S_2N_3Fe_2ClPF_6$	$C_{21}H_{38}S_2N_3Fe_2ClPF_6$	$C_{19}H_{35}S_2N_2Fe_2Cl_2$
Formula weight	674.76	688.78	538.21
Crystal dimensions (mm^3)	0.39 × 0.33 × 0.31	0.53 × 0.33 × 0.32	0.25 × 0.24 × 0.24
Crystal system	Orthorhombic	Orthorhombic	Monoclinic
Space group	Pbca	Pbca	P2(1)/c
a (Å)	16.1521(9)	11.7179(6)	11.7179(6)
b (Å)	17.3762(9)	15.2415(8)	15.2415(8)
c (Å)	20.4850(11)	33.0452(17)	33.0452(17)
α (°)	90.00	90.00	90.00
β (°)	90.00	90.00	95.3012(11)
γ (°)	90.00	90.00	90.00
Volume (Å ^{3})	5749.4(5)	5901.8(5)	2335.60(11)
Z	8	8	4
T (K)	299(2)	295(2)	173(2)
D_{calcd} (g cm^{-3})	1.559	1.550	1.531
μ (mm^{-1})	1.357	1.324	1.658
F (000)	2776	2840	1124
No. of rflns. collected	34478	37751	39653
No. of indep. rflns. / R_{int}	5051 / 0.0445	5071 / 0.0666	4112 / 0.0307
No. of obsd. rflns. [$I_0 > 2\sigma(I_0)$]	3889	3595	3951
Data / restraints / parameters	5051 / 25 / 314	5071 / 15 / 325	4112 / 0 / 244
R_1 / wR_2 [$I_0 > 2\sigma(I_0)$]	0.0618 / 0.1773	0.0797 / 0.1799	0.0521 / 0.1318
R_1 / wR_2 (all data)	0.0799 / 0.1887	0.1161 / 0.1950	0.0537 / 0.1328
GOF (on F^2)	1.026	1.012	1.016
Largest diff. peak and hole (e Å $^{-3}$)	1.259 / –0.631	1.937 / –0.668	2.373 / –1.105

Figure S1. ORTEP diagram of **1**, hydrogen atoms and counterion PF_6^- are omitted for clarity (thermal ellipsoids shown at 50% probability)

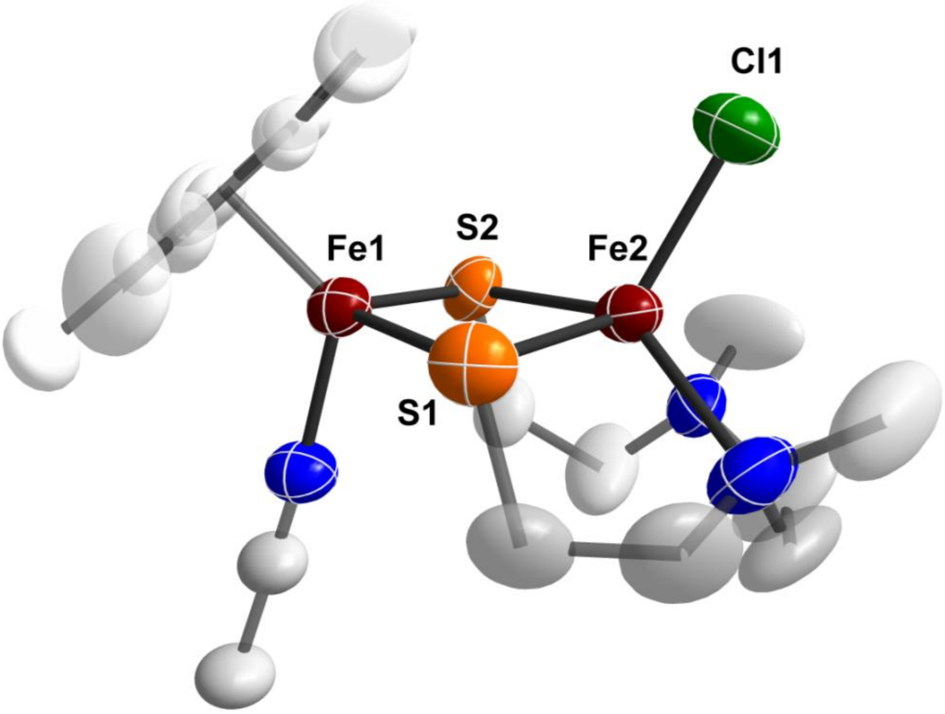

Table S2. Selected bond distances (Å) and bond angles (°) for **1**

Distances (Å)			
Fe1–Fe2	3.115(1)	Fe2–S1	2.401(2)
Fe1–S1	2.280(2)	Fe2–S2	2.442(1)
Fe1–S2	2.259(2)	Fe2–Cl1	2.238(1)
Angles (°)			
Fe1–S1–Fe2	82.89(5)	S1–Fe1–S2	100.61(6)
S1–Fe2–S2	92.29(5)	Fe2–S2–Fe1	83.38(5)
Torsion angles (°)			
S1–Fe1Fe2–S2	170.91(7)	Fe1–S1S2–Fe2	169.64(6)

Figure S2. ORTEP diagram of **2**, hydrogen atoms on carbons (except C1) and counterion PF$_6^-$ are omitted for clarity (thermal ellipsoids shown at 50% probability)

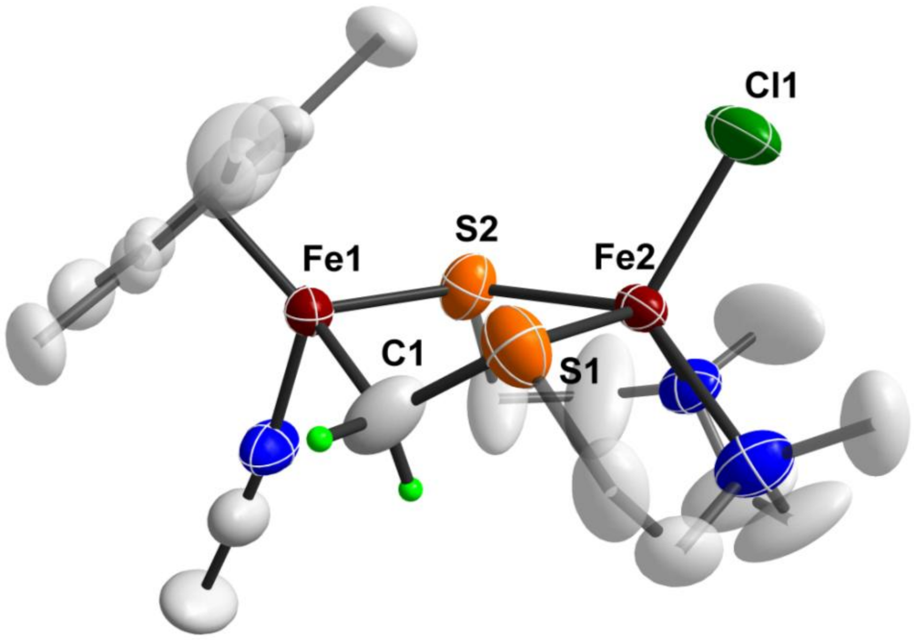

Table S3. Selected bond distances (Å) and bond angles (°) for **2**

Distances (Å)			
Fe1–Fe2	3.822(1)	Fe1–Cl1	2.242(2)
Fe1–C1	2.026(7)	C1–S1	1.712(10)
Fe2–S1	2.437(2)	Fe2–S2	2.428(2)
Fe1–S2	2.220(2)		
Angles (°)			
Fe1–S2–Fe2	110.52(9)	Fe1–C1–S1	114.4(5)
S2–Fe1–C1	93.4(3)	S2–Fe2–S1	88.09(8)
Fe2–S1–C1	104.9(3)		
Torsion angles (°)			
S2–Fe1S1–C1	124.2 (3)	S1–Fe1Fe2–S2	178.76(8)
Fe1–S1S2–Fe2	178.94(7)		

Figure S3. ORTEP diagram of **3**, hydrogen atoms on carbons (except C1) are omitted for clarity (thermal ellipsoids shown at 50% probability)

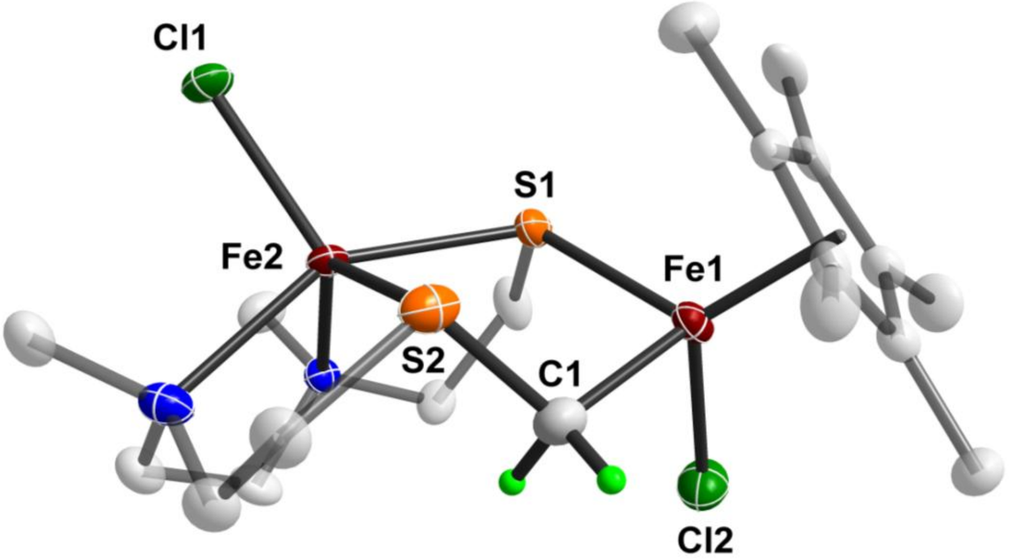

Table S4. Selected bond distances (Å) and bond angles (°) for **3**

Distances (Å)			
Fe1–Fe2	3.862(1)	Fe1–Cl2	2.311(1)
Fe1–C1	2.025(5)	S2–C1	1.789(5)
Fe2–S2	2.456(1)	Fe2–S1	2.395(1)
Fe1–S1	2.304(1)	Fe2–Cl1	2.264(1)
Angles (°)			
Fe1–S1–Fe2	110.56(9)	Fe1–C1–S2	113.4(2)
S1–Fe1–C1	90.89(14)	S1–Fe2–S2	86.67(4)
Fe2–S2–C1	96.54(17)		
Torsion angles (°)			
S1–Fe1S2–C1	123.6(2)	S1–Fe1Fe2–S2	153.97(4)
Fe1–S1S2–Fe2	158.35(4)		

ESI-HRMS

Figure S4. ESI-HRMS of **1** in MeCN, (a) The signal at an *m/z* = 488.0483 corresponds to [**1**−PF_6−MeCN]$^+$. (b) Calculated isotopic distribution for [**1**−PF_6−MeCN]$^+$ (upper) and the amplifying experimental diagram for [**1**−PF_6−MeCN]$^+$ (bottom).

(a)

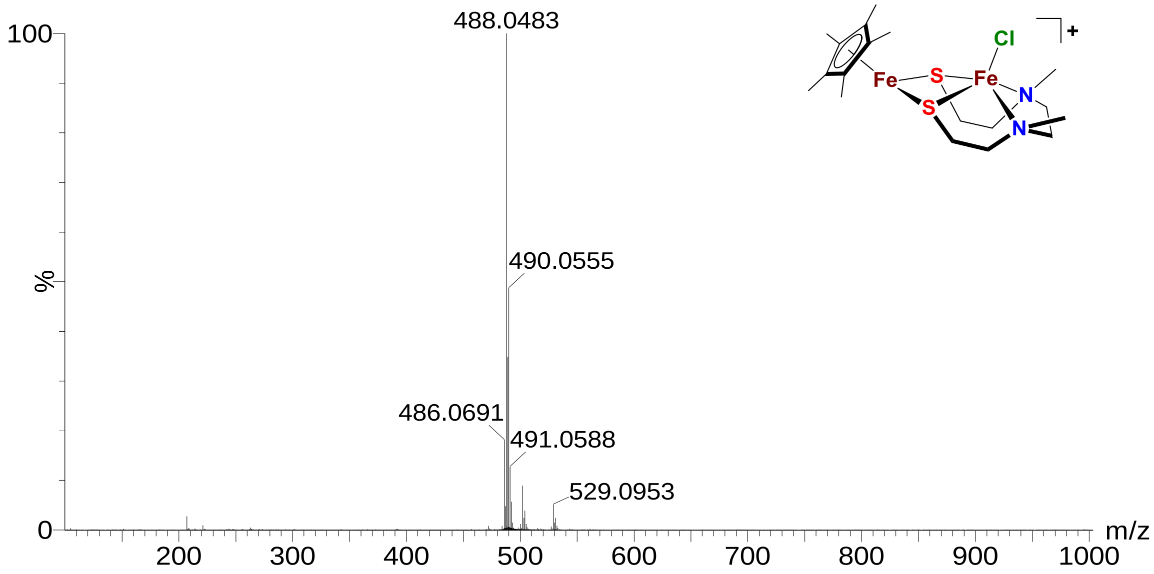

(b)

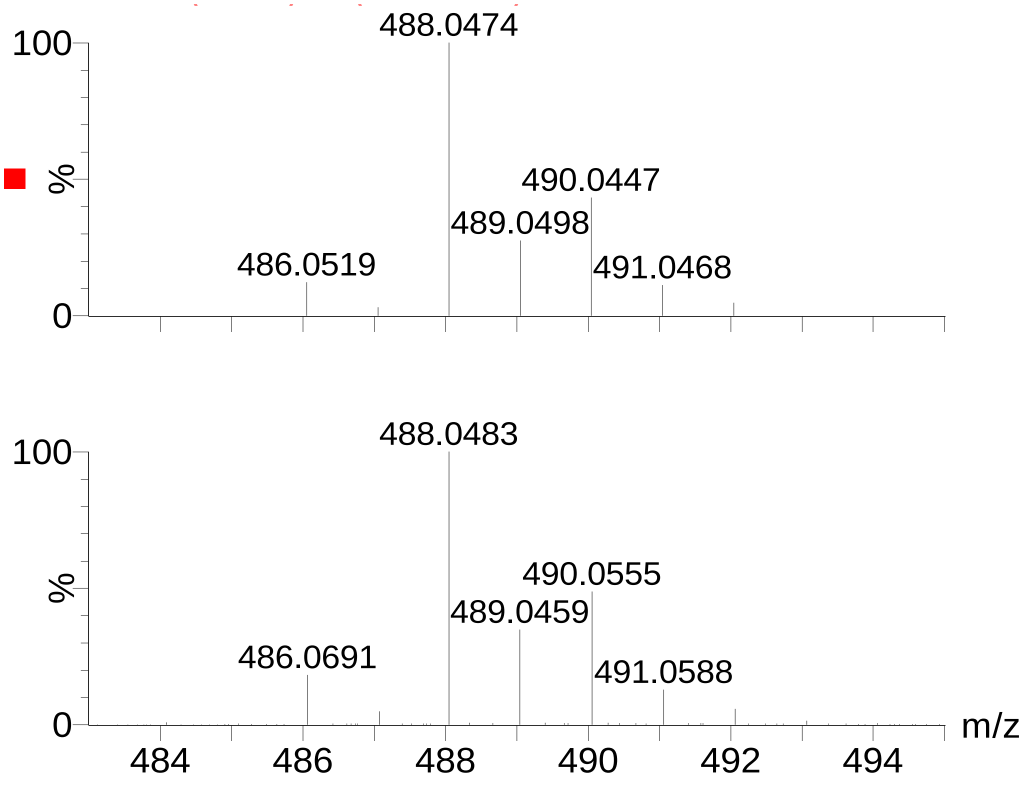

Figure S5. ESI-HRMS of **2** in MeCN, (a) The signal at an m/z = 502.0613 corresponds to [**2**−PF$_6$−MeCN]$^+$. (b) Calculated isotopic distribution for [**2**−PF$_6$−MeCN]$^+$ (upper) and the amplifying experimental diagram for [**2**−PF$_6$−MeCN]$^+$ (bottom).

(a)

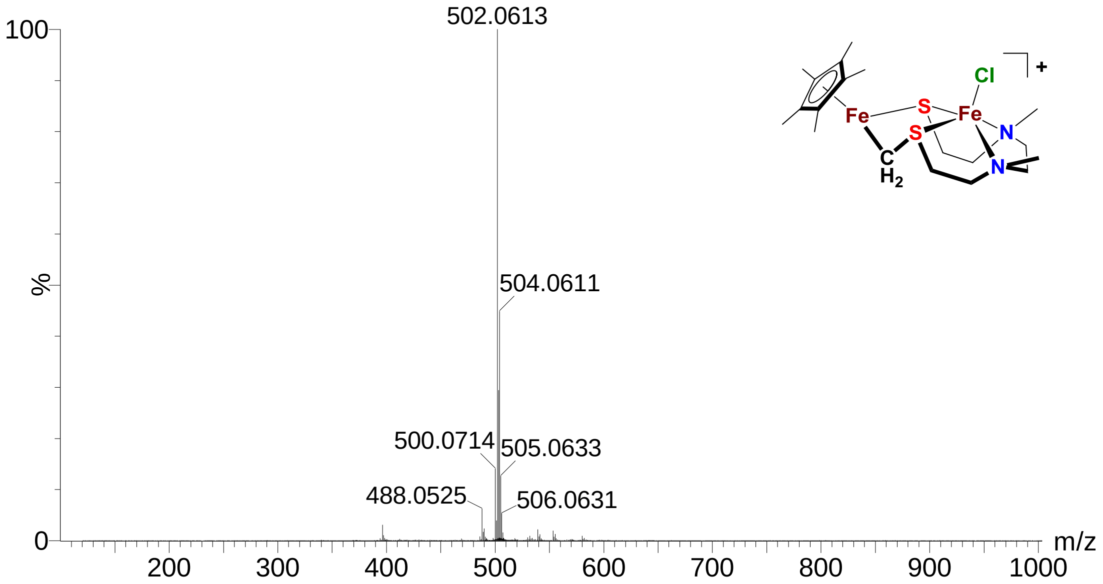

(b)

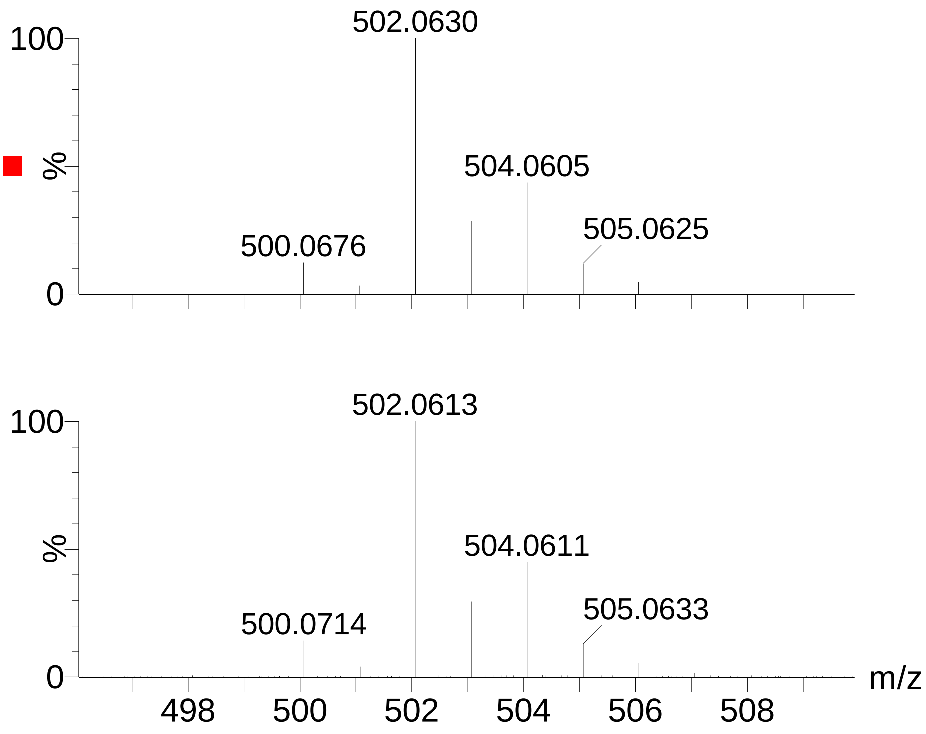

Figure S6. ESI-HRMS of $\mathbf{2}^{\mathbf{CD2}}$ in MeCN, (a) The signal at an *m/z* = 504.0743 corresponds to $[\mathbf{2}^{\mathbf{CD2}}\text{–PF}_6\text{–MeCN}]^+$ (b) Calculated isotopic distribution for $[\mathbf{2}^{\mathbf{CD2}}\text{–PF}_6\text{–MeCN}]^+$ (upper) and the amplifying experimental diagram for $[\mathbf{2}^{\mathbf{CD2}}\text{–PF}_6\text{–MeCN}]^+$ (bottom).

(a)

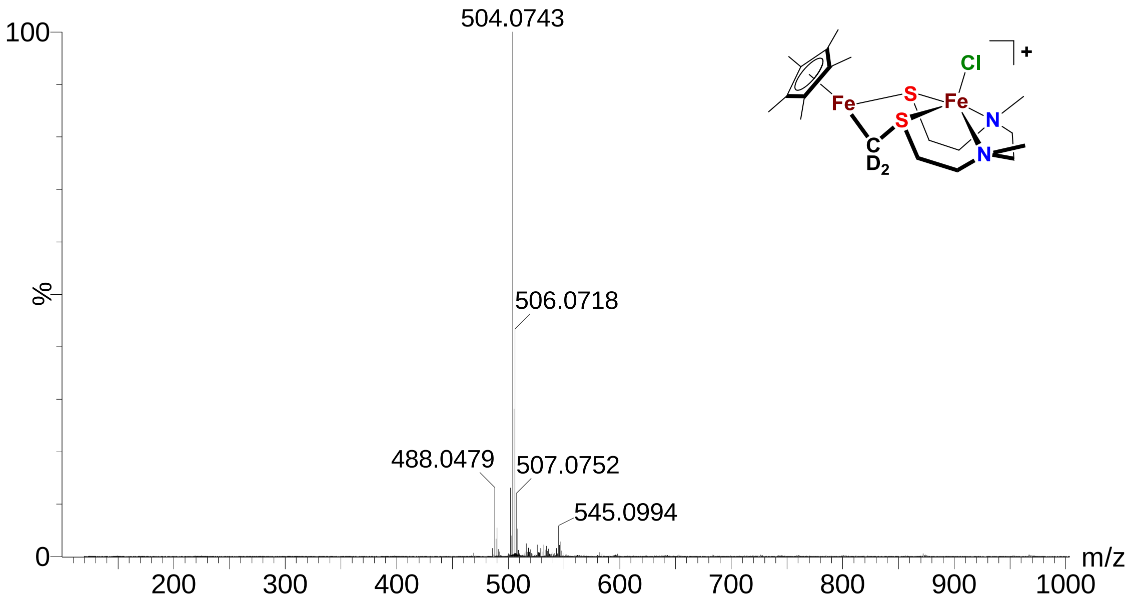

(b)

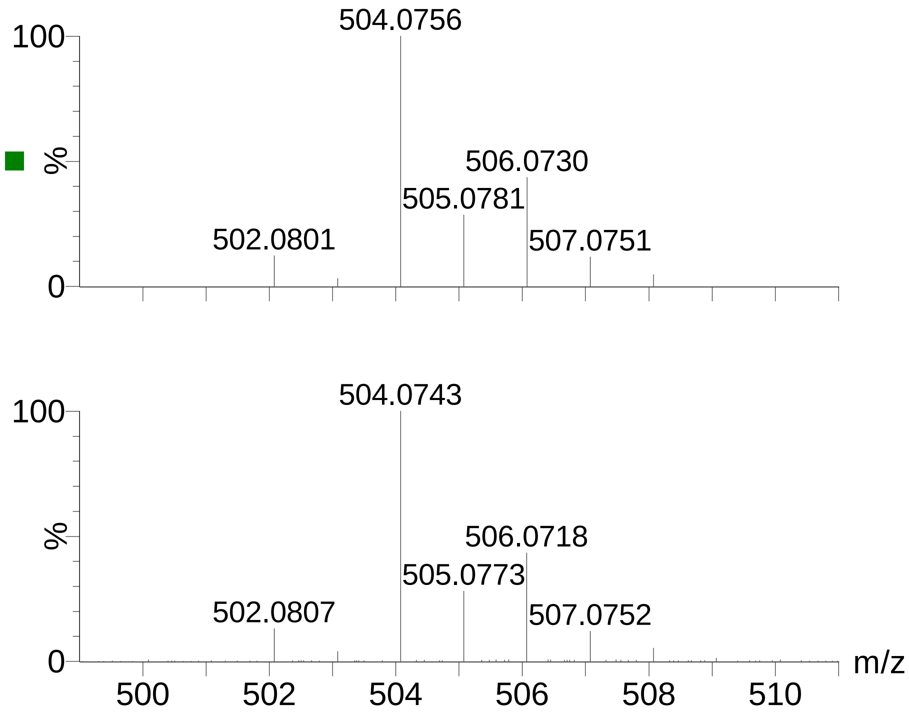

Figure S7. ESI-HRMS of **1'** and **2'** in MeCN, (a) The signal at an *m/z* = 531.9968 corresponds to [**1'**−PF_6−MeCN]$^+$ and 546.0143 corresponds to [**2'**−PF_6−MeCN]$^+$. (b) Calculated isotopic distribution for [**1'**−PF_6−MeCN]$^+$ (upper) and the amplifying experimental diagram for [**1'**−PF_6−MeCN]$^+$ (bottom). (c) Calculated isotopic distribution for [**2'**−PF_6−MeCN]$^+$ (upper) and the amplifying experimental diagram for [**2'**−PF_6−MeCN]$^+$ (bottom).

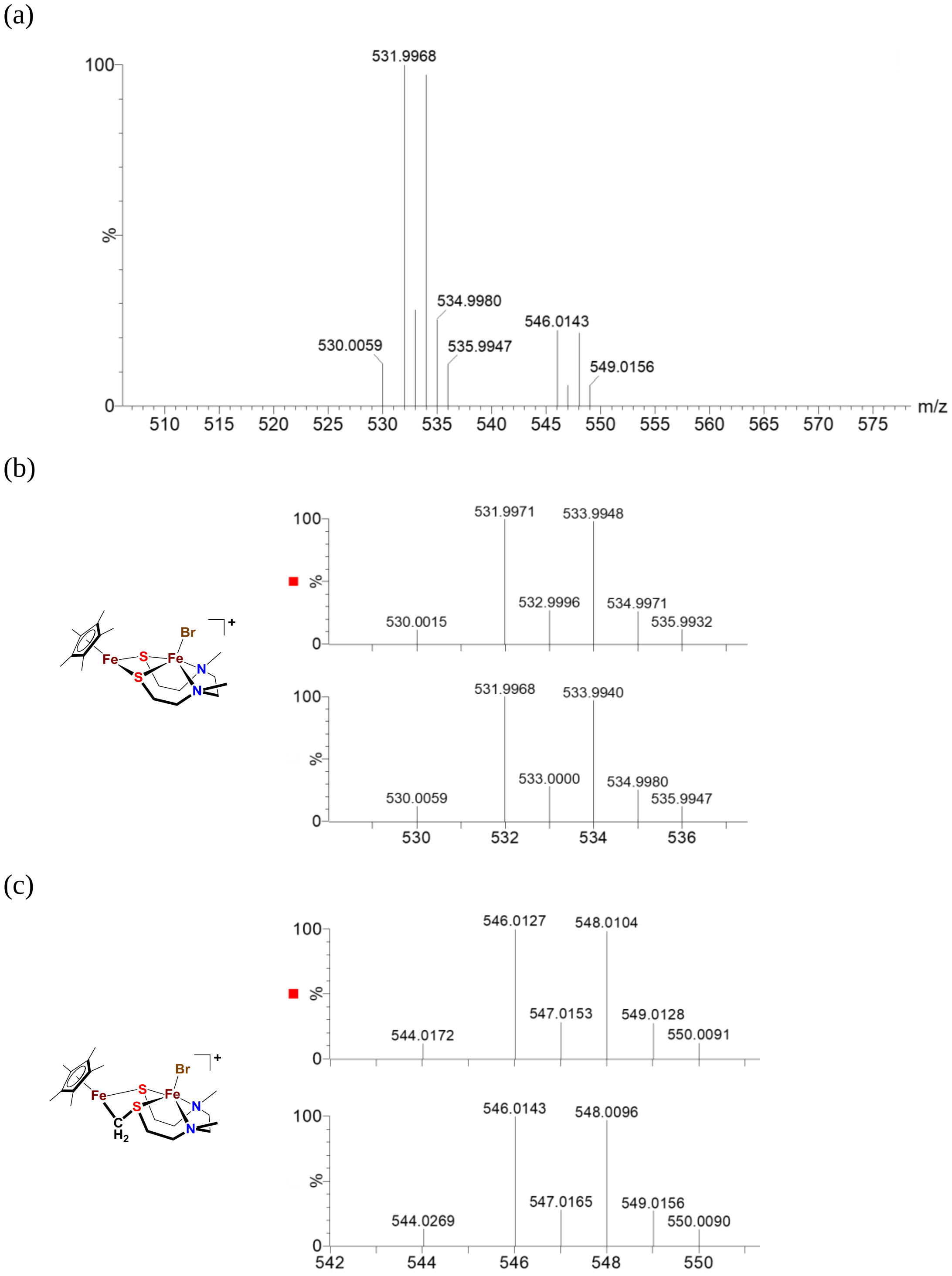

Figure 8. ESI-HRMS of **1''** in MeCN, (a) The signal at an *m/z* = 534.0164 corresponds to [**1''**−PF_6−MeCN]$^+$. (b) Calculated isotopic distribution for [**1''**−PF_6−MeCN]$^+$ (upper) and the amplifying experimental diagram for [**1''**−PF_6−MeCN]$^+$ (bottom).

(a)

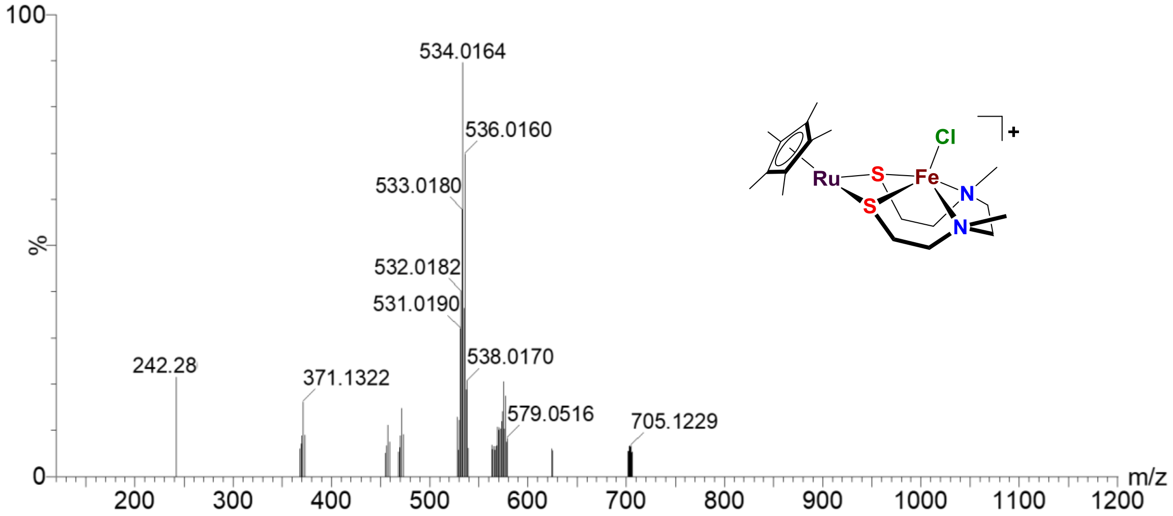

(b)

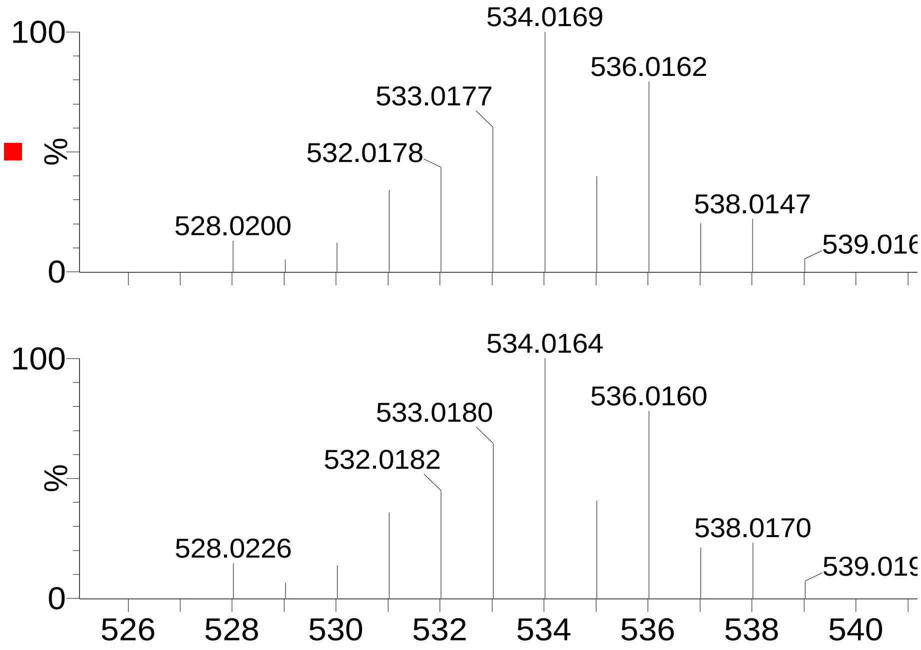

^{1}H NMR Spectra

Figure S9. The ^{1}H NMR spectrum of **1** in CD_3CN

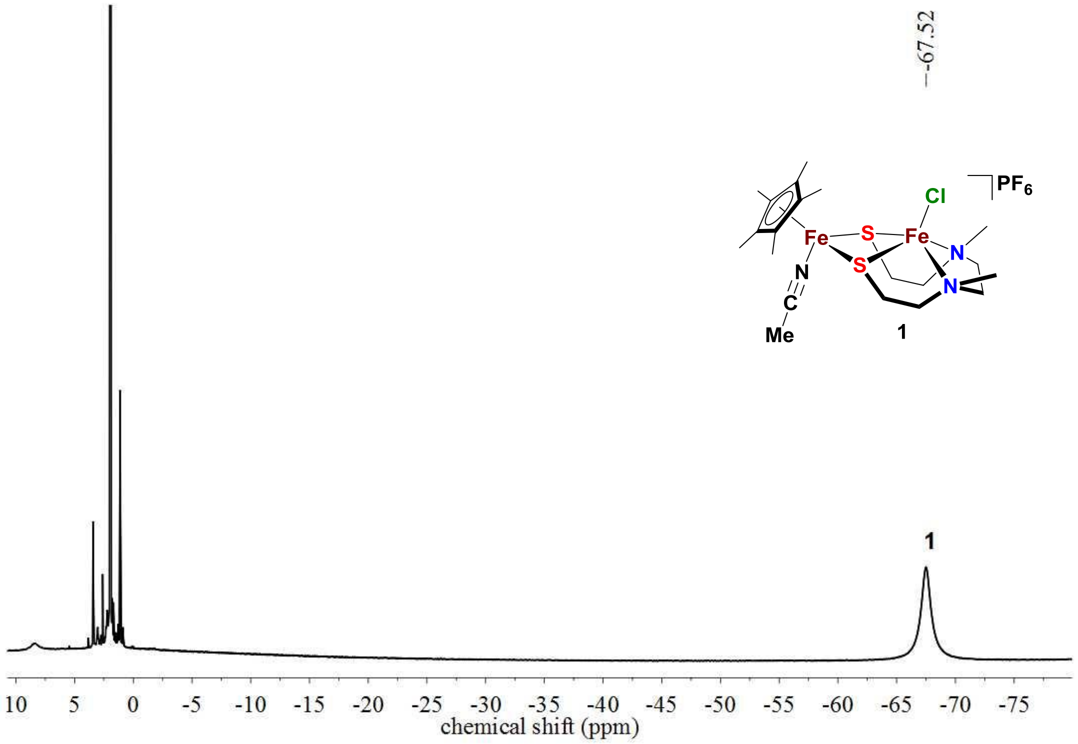

Figure S10. The ^{1}H NMR spectrum of **2** in CD_3CN

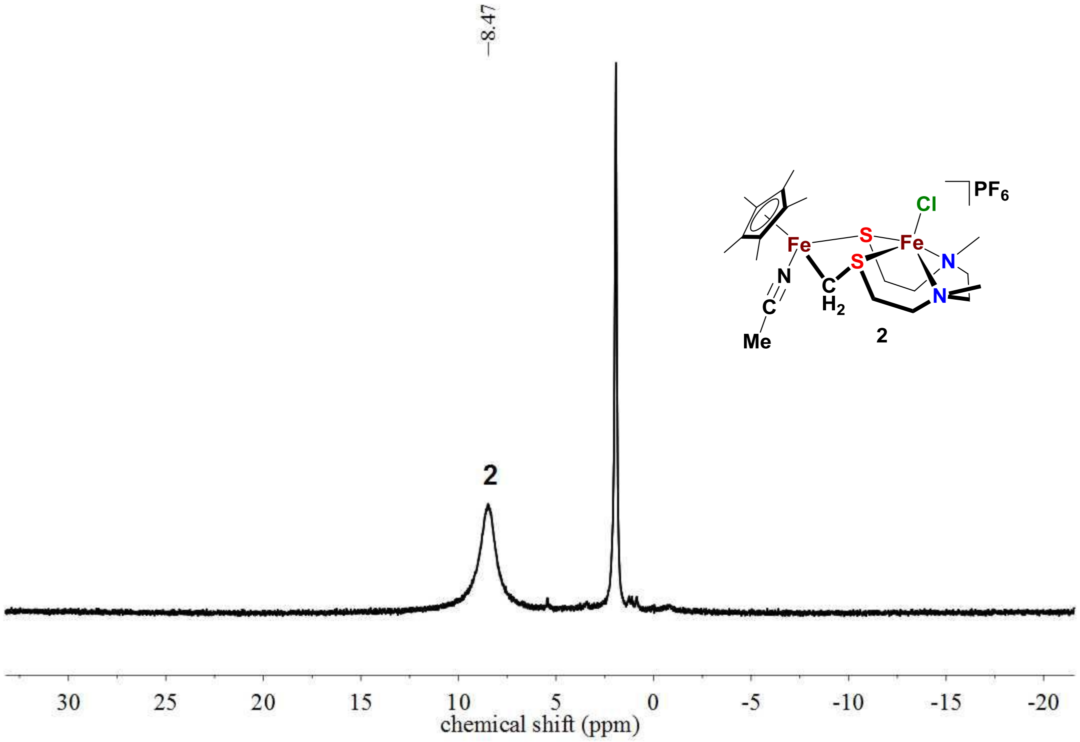

Figure S11. The ^{1}H NMR spectrum of **3** in CD_2Cl_2

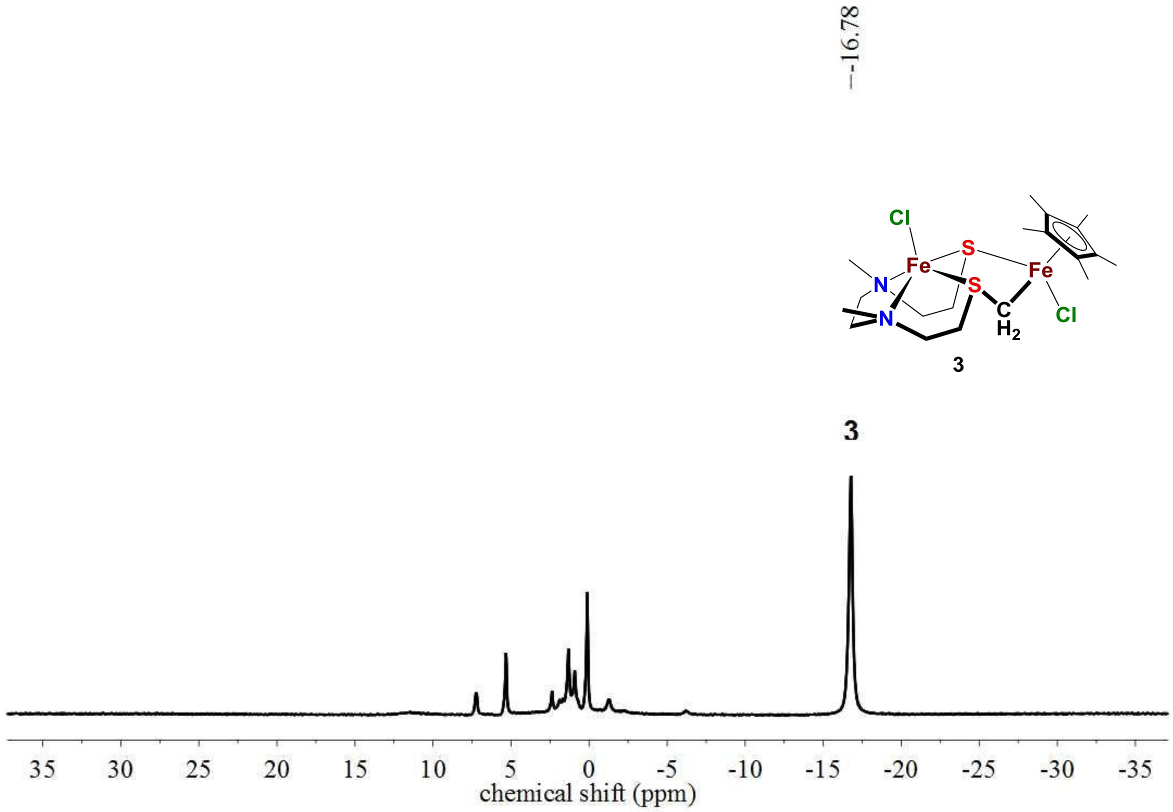

IR Spectra

Figure S12. The IR (film) spectrum of **1**

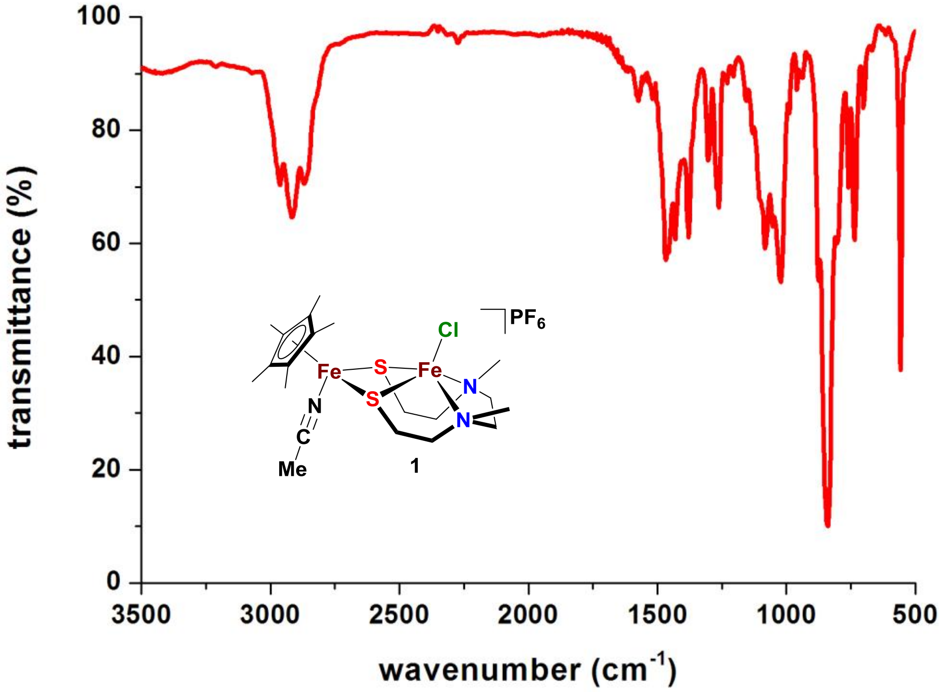

Figure S13. The IR (film) spectrum of **2**

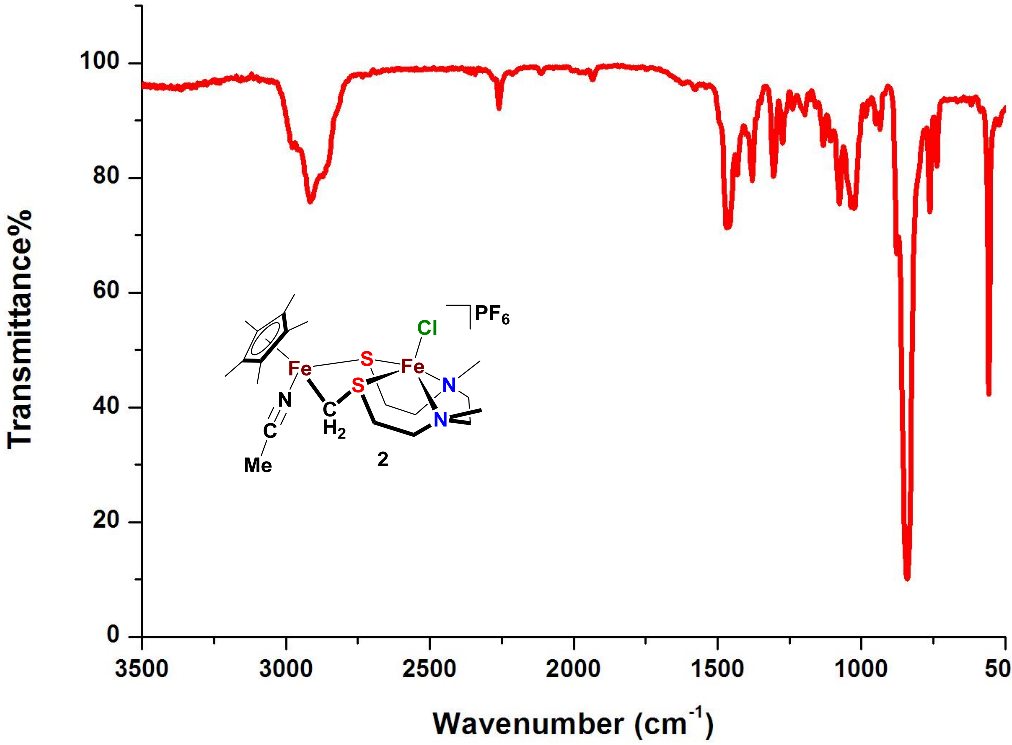

Figure S14. The IR (film) spectrum of **3**

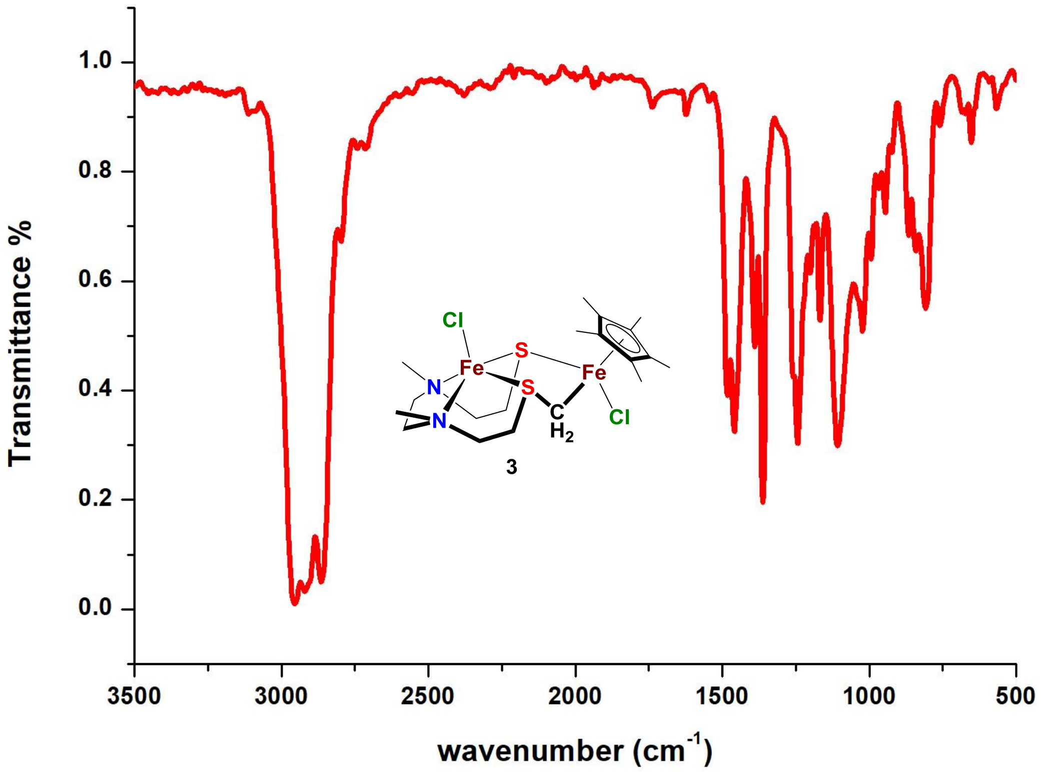

Mössbauer Spectra

Figure S15. ^{57}Fe Mössbauer spectrum of **1**. The data (dots) and best fit (solid line) are shown. The fitting parameters are listed below.

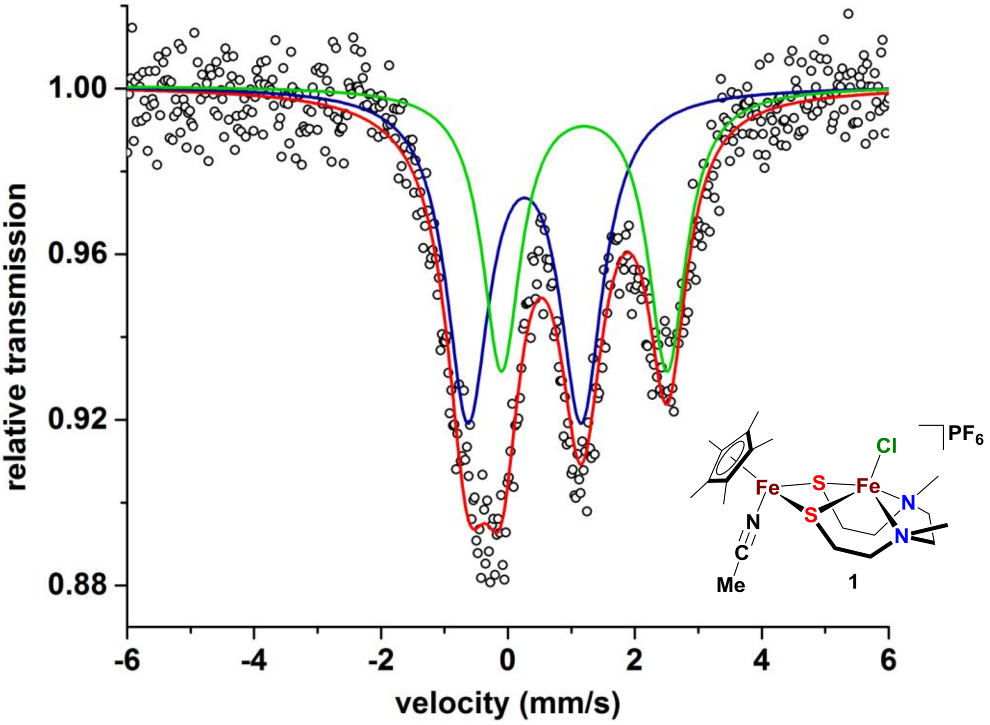

T (K)		δ (mm/s)	ΔE_Q (mm/s)	Γ (mm/s)
80	43.8%	1.20	2.62	0.74
	56.2%	0.26	1.79	0.83

Figure S16. ^{57}Fe Mössbauer spectrum of a mixture of **1** and **2**. The data (dots) and best fit (solid line) are shown. The fitting parameters are listed below.

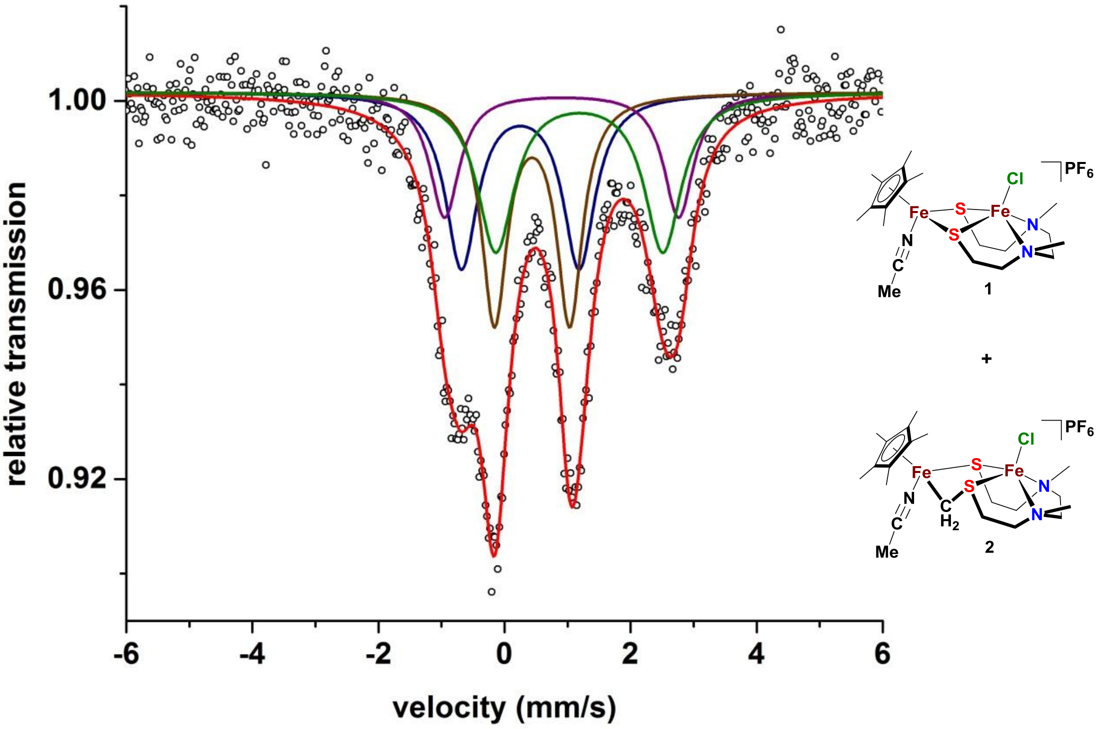

T (K)		δ (mm/s)	ΔE_Q (mm/s)	Γ (mm/s)
80	26.54%	0.25	1.87	0.61
	17.75%	0.91	3.71	0.57
	27.77%	0.44	1.19	0.49
	27.94%	1.18	2.65	0.71

Computational Details

Table S5. Computed relative electronic energies of the cations of **1**, **2** and **3** at different electronic states. The relative electronic energies are given in kcal/mol.

	1	**2**	**3**
E(S = 1/2)	11.7	13.0	8.3
E(S = 3/2)	4.8	0.0	0.8
E(S = 5/2)	0.0	1.7	0.0
E(S = 7/2)	22.1	21.6	13.2

The results show that for **1** and **3**, the S = 5/2 state is the most stable. For **2**, S = 3/2 state is the most stable.

Figure S17. The optimized structure (bond length in Å and angle in degree) of **2**, hydrogen atoms and counterion PF_6^- are omitted for clarity.

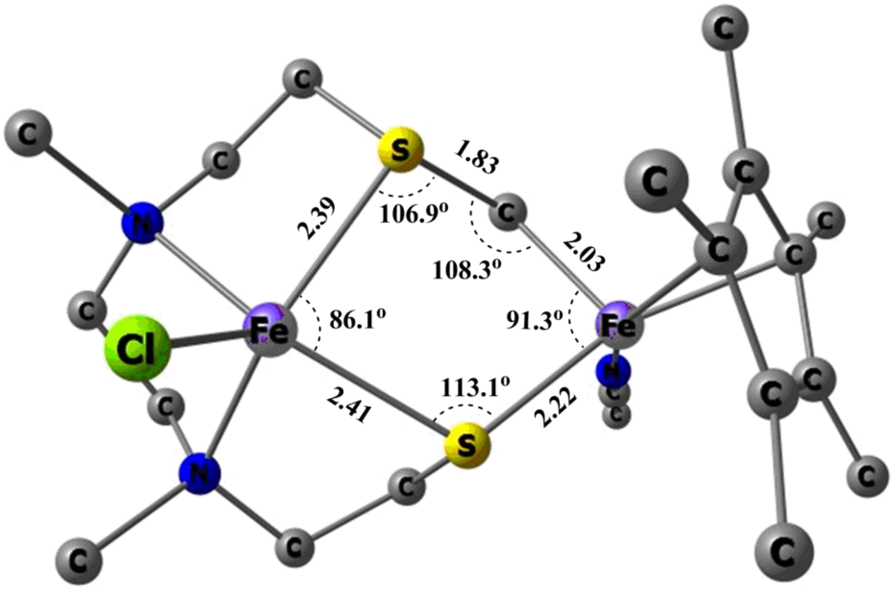

The optimized structure together with some important geometrical parameters is shown in ***Figure S17***. The interatomic distances are excellent in line with experimental ones suggesting the reliability of the method applied.

Table S6. Computed spin population of **1**, **2** and **3** at most stable electronic states[a]

	Fe atoms	**S atoms**	**Cl atom**	**N atoms**
1	4.41	0.28	0.27	0.05
2	2.82	−0.13	0.22	−0.01
3	4.83	0.02	0.22	−0.01

[a] The positive values denote *α* spin electrons and the negative values represent *β* spin electrons.

Figure S18. The spin distribution in the three complexes calculated at the TPSSTPSS level. The purple regions have excess *α* density and the blue areas have excess *β* density. The plot is created by GaussView 5.0.

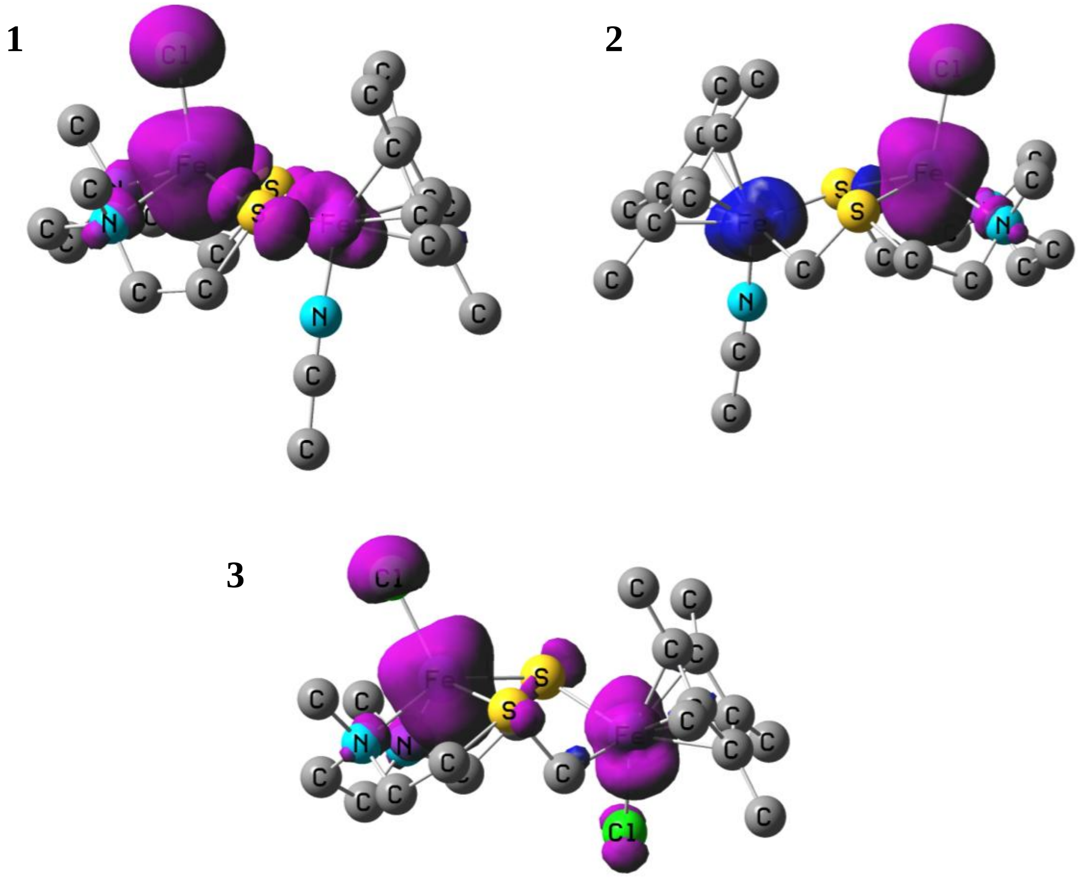

Calculated spin density distribution for the cations of 1, 2 and 3

The spin density was obtained as the difference between the α and β spin contributions. We followed the normal convention that the number of α electrons is considered to be greater than β electrons. ***Table S6*** shows the computed spin density populations at different sites. The spatial spin density distribution for **1**, **2** and **3** obtained at the level of TPSSTPSS is shown in ***Figure S18***. The excess of α spin is mainly found at the central Fe atoms, as suggested by the larger positive spin distribution on the Fe atoms. A notable amount of α spin is also located at the Cl, S and N atoms. The striking feature is the significant excess of β spin on Fe atoms in **2**. The Cp* ring have little spin distribution.